Contact angle hysteresis can modulate the Newtonian rod-climbing effect

Cite as: Phys. Fluids **34**, 093110 (2022); https://doi.org/10.1063/5.0115521
Submitted: 27 July 2022 • Accepted: 30 August 2022 • Accepted Manuscript Online: 01 September 2022 • Published Online: 21 September 2022

Navin Kumar Chandra, Kaustuv Lahiri and Aloke Kumar

Physics of Fluids ARTICLE scitation.org/journal/phf

Contact angle hysteresis can modulate the Newtonian rod-climbing effect

Cite as: Phys. Fluids **34**, 093110 (2022); doi: 10.1063/5.0115521
Submitted: 27 July 2022 · Accepted: 30 August 2022 ·
Published Online: 21 September 2022

Navin Kumar Chandra, Kaustuv Lahiri, and Aloke Kumar[a)]

AFFILIATIONS

Department of Mechanical Engineering, Indian Institute of Science Bangalore, Karnataka 560012, India

[a)]Author to whom correspondence should be addressed: alokekumar@iisc.ac.in

ABSTRACT

The present work investigates the role of contact angle hysteresis at the liquid–liquid–solid interface (LLS) on the rod-climbing effect of two immiscible Newtonian liquids using experimental and numerical approaches. Experiments revealed that the final steady-state contact angle, θ_w, at the LLS interface varies with the rod rotation speed, ω. For the present system, θ_w changes from $\sim 69^\circ$ to $\sim 83^\circ$ when the state of the rod is changed from static condition to rotating at 3.3 Hz. With further increase in ω, the θ_w exceeds 90°, which cannot be observed experimentally. It is inferred from the simulations that the input value of θ_w saturates and attains a constant value of $\sim 120^\circ$ for $\omega > 5$ Hz. Using numerical simulations, we demonstrate that this contact angle hysteresis must be considered for the correct prediction of the Newtonian rod-climbing effect. Using the appropriate values of the contact angle in the boundary condition, an excellent quantitative match between the experiments and simulations is obtained in terms of the climbing height, the threshold rod rotation speed for the onset of climbing, and the shape of the liquid–liquid interface. This resolves the discrepancy between the experiments and simulations in the existing literature where a constant value of the contact angle has been used for all speeds of rod rotation.

I. INTRODUCTION

An interesting non-intuitive behavior is displayed by the interface of two immiscible Newtonian liquids in the presence of a vertically immersed rotating rod. Beyond a certain rod rotation speed, the liquid–liquid interface shows a climbing in the vicinity of the rod. This non-intuitive phenomenon was first reported by Bonn *et al.*,[1] and they named it as the Newtonian rod-climbing effect. The essential criterion for climbing is that the lighter liquid should have higher viscosity; otherwise, a dip is observed instead of a climb.[1,2] The name "rod-climbing effect" comes from a similar phenomenon classically observed at the air–liquid interface of viscoelastic liquids like polymer melts[3] and polymeric solutions.[4–6] Although the stretched interface has a similar shape in both, the Newtonian and the viscoelastic rod-climbing effect, the governing mechanism is completely different. In the case of the viscoelastic liquids, rod climbing happens due to the dominance of the normal stress differences over the centrifugal force. However, in the case of the Newtonian rod-climbing effect, the inertial force due to secondary flows in the heavier liquid provides the necessary driving force for climbing of the interface.[1] This mechanism of secondary flow-driven rising of the liquid–liquid interface is confirmed by previous studies but in a different geometry. For instance, Berman *et al.*[7] did early studies on the upheaval of the liquid–liquid interface in a spinning centrifuge tube. Similar phenomenon was reported by Fujimoto and Takeda[8] in a stationary cylindrical container with a circular rotating lid on top. The particular case of the liquid–liquid interface deformation by a rotating rod is studied by Zhao *et al.*[2] and Bonn *et al.*[1] Zhao *et al.*[2] demonstrated that rods of varied materials (Teflon, PVC, stainless steel) produced comparable magnitudes of climbing height. Based on this observation, the authors suggested that Newtonian rod climbing is mainly hydrodynamic in nature and does not depend on the wetting properties. They also supplemented their experiments with simulations, which show a qualitative match, thereby establishing the fact that the Newtonian rod-climbing effect can be captured numerically through the Navier–Stokes equations using the volume-of-fluid (VOF) approach for multiphase formulation.

The existing literature does not account for the contact angle hysteresis (CAH) at the three-phase contact line (CL) of the liquid–liquid–solid interface in the rod climbing of Newtonian liquids. However, our previous work[6] outlines the role of CAH due to CL pinning, but for an entirely different system of gas–liquid–solid interface in the rod climbing of viscoelastic liquid. Dynamics of a liquid–liquid–solid CL as opposed to gas–liquid–solid CL presents a more complex system because the interaction of the two liquids with the solid surface is comparable.[9,10] In such systems, CAH can be observed

depending upon the roughness and wetting properties of the solid substrate,[11–13] surface energies of different materials,[14] and viscous dissipation due to flow near the three-phase CL.[15,16] The origin of CAH lies in the microscopic phenomena at the molecular level, but its effect is observed at the macroscopic level.[17–19] It is a challenging task to model the moving the contact line, dynamic contact angle, and CAH at the three-phase contact line. It has been extensively studied in the past few decades and still an ongoing area of research.[17–22] Neglecting the CAH in the free surface problems near a solid surface is an oversimplification, and it may lead to wrong predictions.[6,23] In the case of the presence of CAH, the contact angle for a given system can exhibit a range of steady-state values. However, Zhao *et al.*[2] modeled Newtonian rod climbing with a constant contact angle of 90° irrespective of the rod rotation speed, which is not true as we show in the present work. Although Bonn *et al.*[1] emphasized on the importance of the capillary force due to the interface curvature near the rod, they did not scrutinize the role of CAH on the Newtonian rod climbing. In the present work, we provide experimental evidence for the existence of CAH in the Newtonian rod-climbing effect shown by a stratified system of silicone oil and DI water in the presence of a rotating stainless steel rod. The quantitative discrepancy between the numerical and experimental results of Zhao *et al.*[2] can be reconciled by accounting for the change in the contact angle due to CAH. We show that, by using the appropriate value of contact angle prescribed as a boundary condition in the numerical simulations, different aspects of Newtonian rod climbing can be captured precisely. In particular, the climbing height, the threshold rod rotation speed for the onset of climbing, and the shape of the oil–water interface have been used as the quantifying parameters to test the proposed hypothesis.

II. MATERIALS AND METHODS

The experimental setup consists of a vertical steel rod (diameter, $D \sim 10$ mm) inserted into a cubical acrylic tank of edge length 100 mm, with transparent walls as shown in Fig. 1. The rod rotation speed, ω, is controlled precisely with a stepper motor connected at the upper end of the rod. ω is varied from 0 to 650 RPM in steps of 50 RPM. However, in rest of this paper, we report ω in Hertz (Hz) to represent the results in a consistent manner with the existing literature.[1] A magnetic tachometer continuously monitors ω. It is observed that the fluctuations in ω from a constant set value are small ($\pm$ 0.05 Hz) compared to the range and the step increment of ω considered in the present study. Therefore, these fluctuations are neglected, and a constant value of rod rotation speed is reported. Despite a robust arrangement of mechanical bearings and couplings between the rod and the stepper motor, lateral vibrations of the rod is inevitable. However, the amplitude of lateral vibrations at the rod–water–oil interface location is very small ($\sim 150 \pm 25\mu$m) compared to any other relevant length scale of the system. Moreover, the oil–water interface is symmetric in visual observation, suggesting that the lateral vibration of the rod is insignificant for the purpose of present study. To perform the experiments, the empty tank is first set in place with respect to the rod as shown in Fig. 1. Then two immiscible Newtonian liquids are poured into the tank. The heavier liquid is DI water, and the lighter one is silicone oil. DI water is poured first after which silicone oil is poured gently to prevent emulsification. 400 ml of liquid is poured to occupy a liquid column height of 40 mm for each liquid. A clearance of 5 mm is present between the tank bottom and the lower end of the rod. This

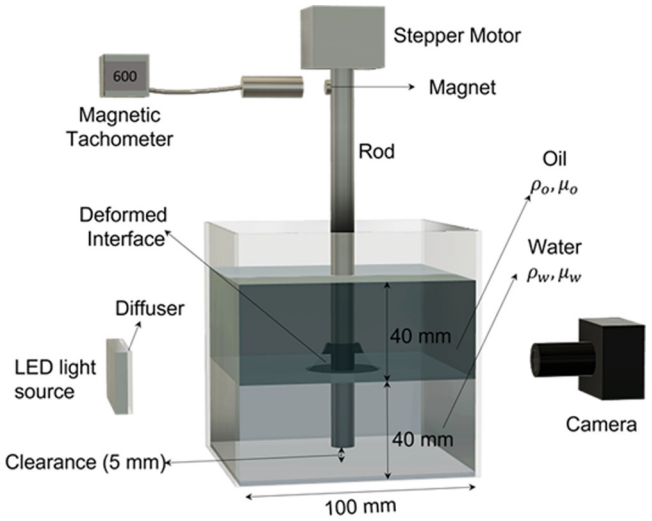

FIG. 1. Schematic diagram of the experimental setup.

geometry ensures that the length of rod dipped in each liquid is more than 25 mm, which is above the limit for the dip length to have any significant effect on the Newtonian rod-climbing phenomenon.[2] The dynamic viscosity of DI water, $\mu_w \sim 1$ mPa s, and silicone oil, $\mu_o \sim 355$ mPa s, are measured using a cone-plate (40 mm diameter) geometry of a rheometer (Anton Paar, MCR 302). Interfacial tension at the oil–water interface, $\gamma \sim 34$ mN/m, is measured by using optical contact angle measuring and contour analysis systems (OCA 15EC, Dataphysics) by creating a pendant drop of water inside an oil bath. Densities of DI water, ρ_w, and silicone oil, ρ_o, are not measured, and their standard values are considered as 998 and 968 kg/m^3, respectively. A DSLR camera (Model: D850, Nikon) and an LED light source are placed at two opposite faces of the liquid tank to track the shape of the oil–water interface near the rod. Images are captured using a macro lens (Sigma 105 mm) in combination with the DSLR camera at high resolution ($\sim 25\,\mu$m/pixel) revealing some unique features of the Newtonian rod climbing, which are not reported in the previous studies. Experiments are performed by slowly ramping ω from the static condition to attain a desired constant value. Sufficient time ($\sim$20 s) is allowed at constant ω for the oil–water interface to achieve a steady stable shape. Finally, the rod rotation is stopped abruptly, and the interfacial meniscus is allowed to recede and occupy the steady static shape. This whole cycle from initial static rod to constant ω and the final static condition is considered as one dataset. A minimum of three datasets have been used for averaging and error analysis. Additionally, we employed particle image velocimetry (PIV) technique to measure the secondary flow velocity field in the meridional plane of water phase. PIV measurements are performed using glass spheres with mean particle size in the range $\sim$9–13 μm and density $\sim$1100 kg/m^3 (purchased from Sigma-Aldrich) as the tracer particle. Meridional plane of interest is illuminated by a laser sheet created with the help of a cylindrical lens. PIV recordings are done at 1000 frames per second using a high-speed camera (Photron Fastcam Mini AX100) in combination with a Navitar zoom lens (6.5X zoom 6000 series). PIV recordings are analyzed using PIVlab software available in MATLAB.

III. NUMERICAL METHODS

A finite volume-based commercial computational fluid dynamics (CFD) code (ANSYS 2021-R2) is employed to perform the numerical simulations. The volume–of-fluid method (which is a surface tracking method) is applied to a fixed Eulerian mesh in order to solve the multiphase system. All the physical properties and variables are shared by the fields, and their volume-averaged values are employed at the interface. The interface is tracked by solving the transport equation for the aqueous phase volume fraction α_w varying between 0 and 1,

$$\frac{\partial \alpha_w}{\partial t} + \boldsymbol{u} \cdot \nabla \alpha_w = 0, \tag{1}$$

where $\boldsymbol{u}$ stands for the velocity field and t for time. A single set of the Navier–Stokes equations was solved for both the fluids,

$$\frac{\partial \rho}{\partial t} + \nabla \cdot \rho \boldsymbol{u} = 0, \tag{2}$$

$$\frac{\partial \rho \boldsymbol{u}}{\partial t} + \nabla \cdot \rho \boldsymbol{u}\boldsymbol{u} = -\nabla p + \rho \boldsymbol{g} + \nabla \cdot \mu(\nabla \boldsymbol{u} + \nabla \boldsymbol{u}^T) + F_\sigma. \tag{3}$$

The density is denoted by ρ, p stands for the pressure field, $\boldsymbol{g}$ stands for the gravitational acceleration vector, μ is the dynamic viscosity, and $\boldsymbol{F}_\sigma$ stands for the surface tension force, which is treated as a body force. Equations (2) and (3) depend on the volume fractions through the characteristics of the density and viscosity. The volume-weighted value of the properties is used in the computational cells having both of the phases,

$$\rho = \alpha_w \rho_w + (1 - \alpha_w)\rho_o, \tag{4}$$

$$\mu = \alpha_w \mu_w + (1 - \alpha_w)\mu_o, \tag{5}$$

where the subscripts o and w stand for oil and water, respectively. The wall adhesion model is also employed which allows for defining the contact angle by taking the input parameter θ_w from the user. The corresponding equation for the normal vector, $\boldsymbol{n}$, of the interface adjacent to the wall is given by

$$\boldsymbol{n} = \boldsymbol{n_w} \cos(\theta_w) + \boldsymbol{n_t} \sin(\theta_w), \tag{6}$$

where $\boldsymbol{n_w}$ is the normal vector to the wall, $\boldsymbol{n_t}$ is the tangential vector to the wall, and θ_w is the wall adhesion angle. θ_w is an input based on experimental observations if $\theta_w < 90^\circ$ and is obtained through an iterative process in case $\theta_w \geq 90^\circ$. This provides a method for modulating the curvature, κ, of the interface in the cells nearest to the rod such that

$$\boldsymbol{n} = \frac{\nabla \alpha_w}{|\nabla \alpha_w|}, \tag{7}$$

$$\kappa = \nabla \cdot \boldsymbol{n}. \tag{8}$$

The surface tension force term is evaluated as follows:

$$\boldsymbol{F}_\sigma = \sigma_a \left(\frac{\kappa \nabla \alpha_w \rho}{\frac{\rho_w + \rho_o}{2}} \right). \tag{9}$$

The effect of θ_w is incorporated into the momentum conservation equation [Eq. (3)] through the $\boldsymbol{F}_\sigma$ term. Because this term depends upon the curvature, κ and hence the normal vector, $\boldsymbol{n}$ of the liquid–liquid interface near the rod [Eq. (8)], which in turn depends upon the θ_w [Eq. (6)]. The $\boldsymbol{F}_\sigma$ term captures the force due to the surface tension, and it is mathematically modeled by the continuum surface force model.[24] The equations discussed in this section are dependent on the volume fractions of each fluid within the cell. Further details pertaining to the simulations are provided in the supplementary material (Note S1).

IV. RESULTS AND DISCUSSION

In the present setup, as the rod is set to rotate at a constant speed, the oil–water interface achieves a stable steady-state profile after few seconds of initial transience. Figures 2(a)–2(e) (Multimedia views) present the steady-state interface shape for different rod rotation speeds. A stable shape of interfacial profile is observed only below a maximum rod rotation speed, ω_{max} (~10 Hz for the present case). Beyond this speed, instead of a stable interface, water-in-oil emulsion is formed through sheet breakup and ring instability as shown in Fig. 2(f) (detailed discussion in the later section). The present study is mainly

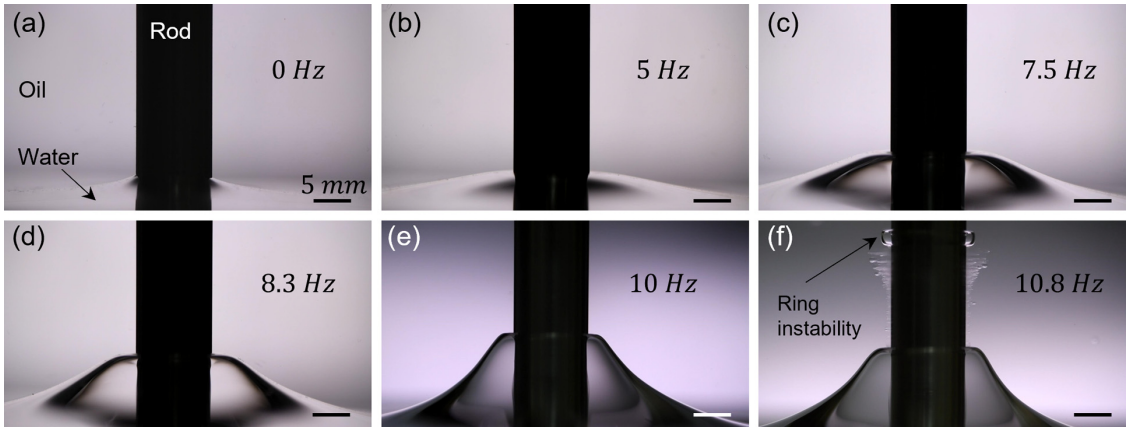

FIG. 2. (a)–(e) Steady-state profile of oil–water interface near the rod rotating at 0, 5, 7.5, 8.3, and 10 Hz, respectively. (f) Emulsification and ring instability at $\omega = 10.8$ Hz. Multimedia view: https://doi.org/10.1063/5.0115521.1

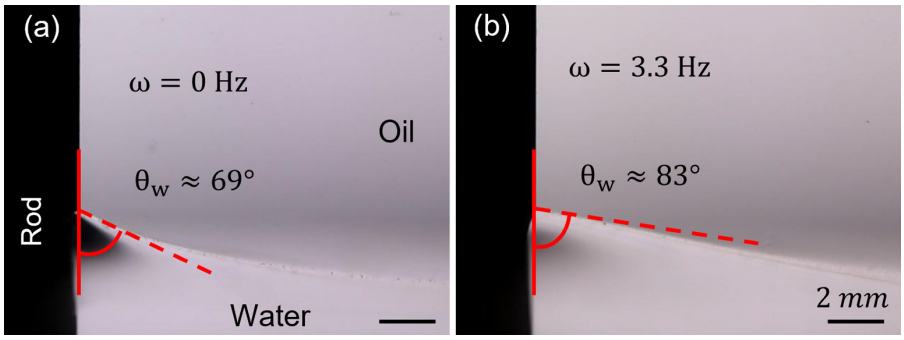

FIG. 3. Right half of the stable interfacial profile near the rod showing the presence of CAH at the oil–water–rod interface. CAH can be observed by comparing the contact angle, θ_w, for (a) static rod, and (b) rod rotating at 3.3 Hz. Multimedia view: https://doi.org/10.1063/5.0115521.2

focused on the regime $\omega \leq \omega_{max}$ where stable interfacial profile is observed.

The existing literature on the rod climbing of Newtonian liquids does not elaborate on the effects of contact angle and assumes that it has a constant value of 90°. Recently, Chandra *et al.*[6] have shown that the CAH due to the pinned CL plays an important role in modulating the rod-climbing effect of viscoelastic liquids. Similar observations are made in the present study for the rod climbing of Newtonian liquids. The contact angle, θ_w, at the three-phase CL of oil–water–rod interface is neither constant nor necessarily 90° as shown in Fig. 3 (Multimedia view). For the materials considered in the present condition, $\theta_w \approx 69°$ when the rod is in static condition [Fig. 3(a)]. As the rod is set to rotate at some constant frequency, the oil–water interface tries to go upward to balance the inertial force due to secondary flows in the lower liquid.[1] Here, we observed that this inertial force is manifested not only in terms of vertical displacement of the oil–water interface but also in terms of the change in θ_w [Fig. 3(b)]. There is a gradual increase in θ_w with increasing speed of rod rotation. For ω up to 3.3 Hz, θ_w is less than 90°, and it is experimentally observable as shown in Fig. 3. With further increase in ω, θ_w becomes greater than 90°. For the case of $\theta_w > 90°$, the three-phase CL is hidden behind the deformed interface, and it cannot be imaged due to the lensing action of the bulged liquid meniscus. Experiments at even higher frequencies reveal the existence of a very thin film of oil between the climbed interface and the rod as shown in Fig. 4. This suggests the possibility that the three-phase CL always remains pinned at its initial position [refer to the schematic in Fig. 4(b)] throughout the course of the rod-climbing experiments, and the observed climb occurs in a region of liquid slightly away from the rod surface. In such a scenario [Fig. 4(a)], it becomes difficult to define and measure the contact angle formed at the actual location of the three-phase CL. Therefore, we define an apparent contact angle, θ_{app}, which is the angle that the oil–water interface appears to make with the rod just before experiencing an almost singular dip [Fig. 4(b)]. θ_{app} can also be thought as the contact angle that the oil–water interface appears to make with the rod surface if the thin film of oil is neglected. θ_{app} is used in place of θ_w in the simulations for the cases of the rod angular frequencies, where $\theta_w \geq 90°$ in the experiments. The detailed methodology adopted in the present work for supplementing the experimental results with simulations is illustrated in the form of a flow chart in Fig. 5. Process is straightforward for lower rod rotation frequencies where $\theta_w < 90°$. In these cases, the input value of θ_w in simulations is directly obtained from the experimental images. For the cases where $\theta_w \geq 90°$, we use the apparent contact angle, θ_{app}, in place of θ_w. θ_{app} cannot be measured from the experimental images due to the hindrance of the bulged meniscus. Therefore, it has been used as a fitting parameter in the numerical simulations, and its value is iterated in steps of 5° starting from 90° to match the climbing height obtained from the corresponding experiment. Step size of 5° is chosen because any smaller change in θ_{app} leads to a change in the climbing height smaller than the present grid resolution of 1 mm (keeping all other variables fixed). In principle, one can consider an arbitrary small step size of θ_{app} and very fine meshing in simulations to get more accurate results. However, to reduce the computational cost, a step size of 5° in the iteration of θ_{app} is considered. The chosen step size and grid

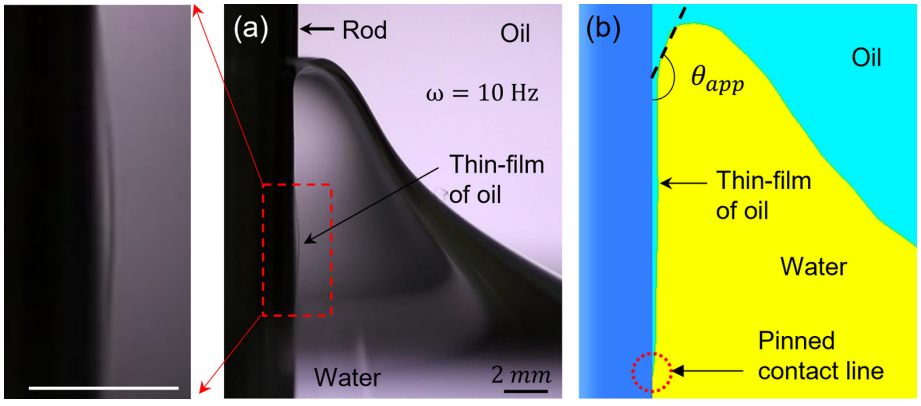

FIG. 4. Topology of the steady-state interface in the vicinity of the rod rotating at high frequencies ($\omega > 5$ Hz). (a) Experimental image showing thin film of oil trapped between water and the rod surface at $\omega = 10$ Hz. (b) Schematic showing macroscopic contact angle θ_{app} at the location of apparent contact between the rod and the oil–water interface, if the thin oil film is neglected.

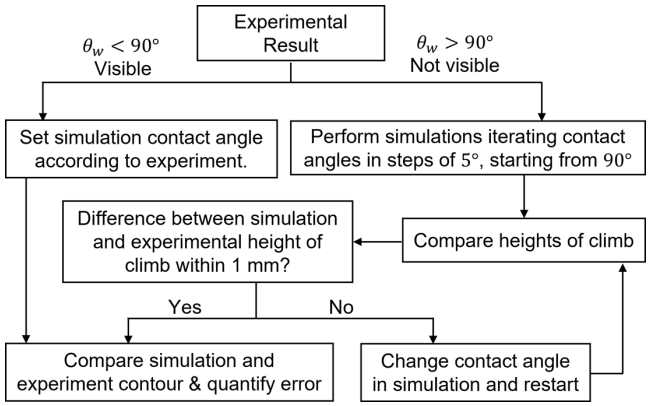

FIG. 5. Flowchart illustrating the methodology of the present work.

resolution are sufficient to identify the essential physics of the present work, that is, to identify the role of CAH in the rod climbing of Newtonian liquids. Once the suitable θ_{app} is known, contour of simulated interfacial profile is compared with experiments and error is estimated. The values of input contact angle at different ω as used in numerical simulations are shown in Fig. 6. For $\omega \leq 3.3$ Hz, the value of θ_w is less than 90° and the presented values have been obtained directly from the measurements using the experimental images. The error bar represents the standard error of three repeated experimental runs. For $\omega > 3.3$ Hz, the value of θ_w goes beyond 90°, which cannot be measured experimentally; therefore, θ_{app} has been used in place of θ_w. Since the simulation is performed by iterating the θ_{app} in steps of 5°, the gray shaded region (Fig. 6) represents the region of uncertainty.

It is worth noting that in the process of defining θ_{app}, the thin film of oil between the rod surface and the oil–water interface is neglected. This thin-film formation is purely an interfacial phenomenon, which occurs due to the interplay of the energies among the water–oil, water–rod, and oil–rod interfaces.[25,26] Therefore, even if the film is neglected in the numerical simulation, there is no significant change in the hydrodynamics of the problem. To probe this further, velocity field of secondary flows in meridional plane of water phase is measured using particle image velocimetry (PIV) technique. This showed a satisfactory match with the flow field obtained from the numerical simulations as shown in Fig. 7. Here, the presence of the bulged meniscus, glare from the rod surface due to laser illumination, and limited field of view did not allow us to perform the PIV measurements near the rod. Therefore, PIV data are shown (Fig. 7) only for a region away from the rod. The match of secondary flow field between experiment and simulation supports our hypothesis that the main physics of the Newtonian rod climbing remains unaffected even if the thin oil film is neglected. The effect of this thin film is indirectly captured in the simulations by virtue of the θ_{app}, which was implicitly kept as 90° in the simulations of Zhao *et al.*[2]

The present study shows that θ_w plays an important role in the rod-climbing effect of Newtonian liquids. By providing the appropriate values of θ_w (from Fig. 6) as a boundary condition, different aspects of the Newtonian rod-climbing effect can be captured properly in the numerical simulations. A visual comparison of simulated and experimental interfacial profiles for different rod rotation speeds is shown in Fig. 8. The present work investigates the effect of θ_w in terms of the climbing height, the threshold rod rotation speed for the onset of climbing, and the interfacial profile. Discussion on each aspect is provided in Subsections IV A and IV B.

A. Climbing height and threshold rod rotation speed

It is already shown that the climbed interface experiences a sharp dip extremely close to the rod (Fig. 4); therefore, climbing height cannot be defined in terms of the vertical displacement of the three-phase CL on the rod surface as done in our previous work.[6] Here, we define the climbing height, H, as the vertical distance between the points of maximum elevation of the steady-state interface at a given ω and the static condition as shown in Fig. 9. The climbing heights at different ω obtained from experiments and simulation are shown in Fig. 10. Simulation results are shown for two different cases: first, assuming a flat meniscus near the rod surface, that is, $\theta_w = 90°$ as used in the existing literature[2] and second, by using the corrected value of θ_w (from Fig. 6) as proposed in the present study. It is clear from Fig. 10 that, if

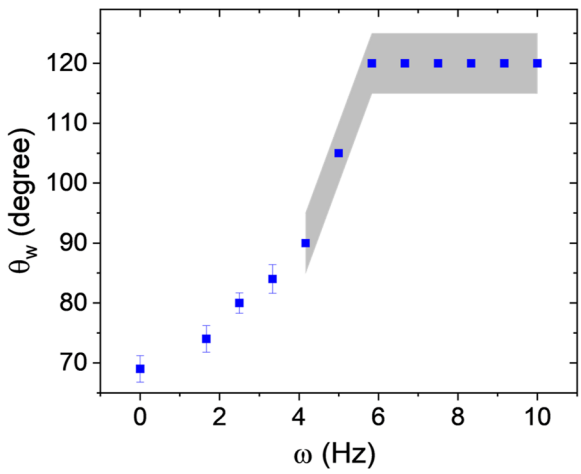

FIG. 6. Variation of the input contact angle with the angular frequency of the rod. Standard error in the case of $\theta_w < 90°$ is obtained from the experiments. For $\theta_w \geq 90°$, there is an uncertainty of 5° represented by the shaded region.

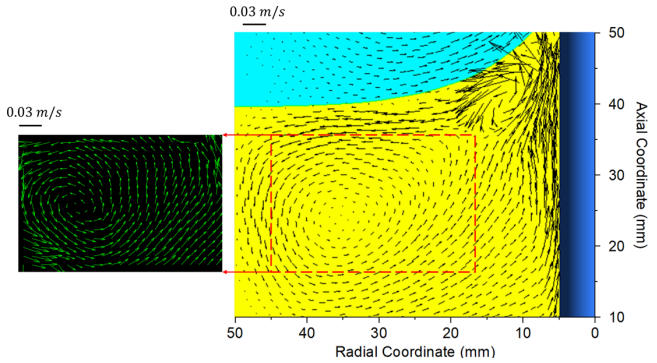

FIG. 7. Velocity field in the meridional plane of the water phase obtained from experiments using PIV (left) and from simulations (right) at $\omega = 10$ Hz for the geometry used in the present work. Red box indicates the region of interest for PIV.

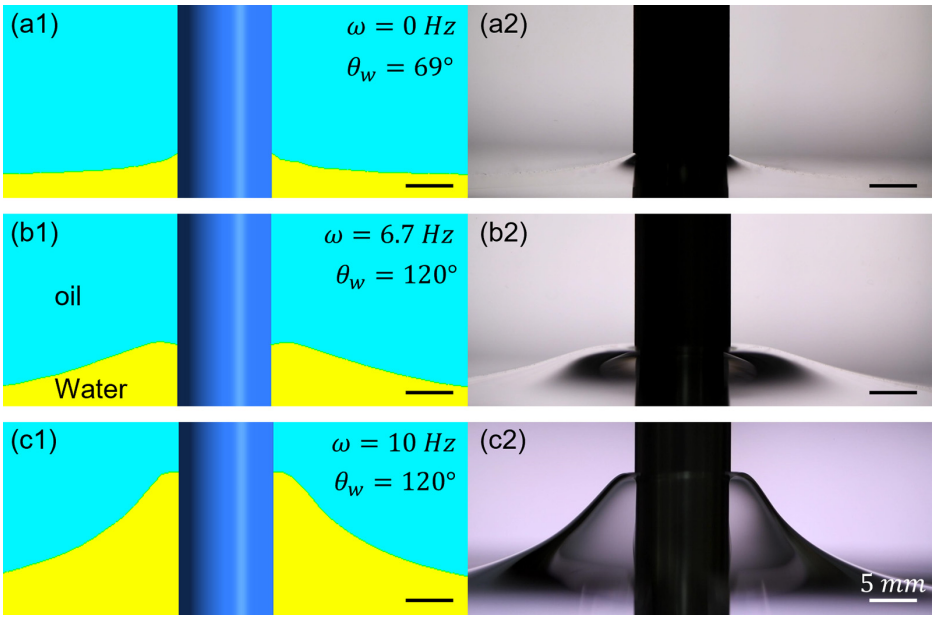

FIG. 8. Stable interfacial profile obtained from simulations (a1)–(c1) and corresponding experiments (a2)–(c2) for rod rotation speeds of 0, 6.7, and 10 Hz, respectively.

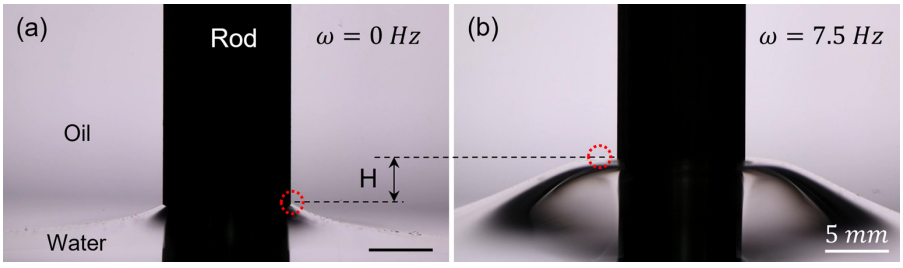

FIG. 9. The stable interfacial profile when the rod is (a) in static condition and (b) rotating at $\omega =$ 7.5 Hz. The height of climb of the interface is denoted by H. Red circle indicates the maximum elevation point of the interfacial profile.

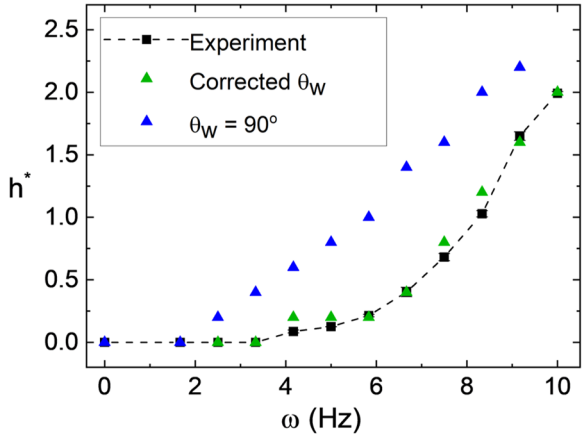

FIG. 10. Variation of the simulation and experimental non-dimensional climbing height, $h^* = \frac{H}{R}$, with the angular frequency of the rod.

a constant value of $\theta_w = 90°$ is considered, that is, the CAH is ignored, then the climbing height obtained from simulation deviates significantly from the experimental values. Also, the threshold rod rotation speed, ω_{th}, for non-zero climbing is predicted to lie between 1.67 and 2.5 Hz, whereas zero climbing is observed even at 3.3 Hz in the experiments. Accounting for the CAH and hence by using the appropriate value of θ_w, the climbing height as well as ω_{th} is predicted properly in the simulations. In the existing literature, ω_{th} is attributed to the critical rod rotation speed for the onset of secondary flows due to Taylor–Couette instability in the heavier liquid.[1] The present study shows that ω_{th} is the rod rotation speed required not just for the onset but to produce the secondary flows strong enough to either overcome the pinning force or to increase the θ_w beyond 90°, whichever is achieved earlier. It should be noted that, for $\omega > 3.3$ Hz, the value of θ_w goes beyond 90° and $\theta_w = \theta_{app}$ is chosen in such a way that the simulated climbing height matches with the experiments. In such cases, the veracity of the proposed mechanism is ascertained by looking at the match of interfacial profiles obtained from simulation and experiments.

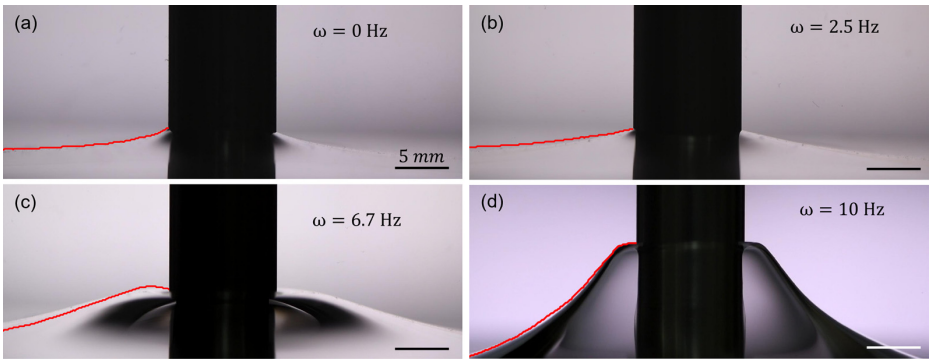

FIG. 11. Match of the steady-state interfacial profile obtained from experiments and simulation (red contour) at different rod rotation frequencies: (a) 0, (b) 2.5, (c) 6.7, and (d) 10 Hz.

B. Interfacial profile

Figure 11 presents the interfacial profile obtained from simulation (red curve) overlapped on the experimental images. For $\omega \leq 3.3$ Hz, the value of θ_w is less than 90°, which is measured directly from the experimental images. Providing these measured values of θ_w as input to the simulations, a proper prediction of climbing height (Fig. 10) and interfacial profile is obtained [Fig. 11(a) and 11(b)]. For $\omega > 3.3$ Hz, the value of $\theta_w = \theta_{app}$ is chosen to match simulation climbing height with the experiments. For the same value of $\theta_{app,}$ a good agreement is found between the experiments and the simulated interfacial profile [Fig. 11(c) and 11(d)]. It is worth noting that the contact angle obtained from the output of the simulation is slightly different from the value provided as an input [120° for Figs. 11(c) and 11(d)]. The reason for this lies in the linear interpolation of the geometric reconstruction scheme to reconstruct the interface (refer to supplementary material Note S2). The error in the match between the experimental and the simulated interfacial profile is within a root mean square value of 0.6 mm for all ω considered in the present study. This error is calculated by taking the root mean square of the vertical deviation between simulation and experimental interfaces at 1000 equally spaced radial locations spanning from the rod surface to $4.5R$ (R being the rod radius). Details of error estimation procedure are provided in the supplementary material (Note S3). It is clear from Figs. 10 and 11 that the modification of θ_w captures the interface deformation both qualitatively and quantitatively. This reinforces the fact that, neglecting the thin oil film present between the deformed interface and the rod, does not lead to any loss of the physics of the problem if θ_w is properly accounted for. Another interesting observation is that the simulation predicts an unstable interface at $\omega = 10$ Hz for $\theta_w = 90°$ [Fig. 12(a)], whereas $\theta_w = 120°$ predicts stable interface at the same rotation frequency [Fig. 12(b)], which matches perfectly with the experimental observation [Fig. 11(d)]. This further supports our claim that the contact angle must be corrected to properly model the Newtonian rod-climbing effect.

C. Trend of θ_w with ω

It is observed that the variation of θ_w with ω shows an interesting trend (Fig. 6). There is an initial increment and then saturation of θ_w with increasing ω, and this can be explained by accounting for the observed thin film of oil. Figure 13 shows the schematic of interfacial profile corresponding to a different rod rotation speed, $\omega_{i,}$ and respective contact angle, $\theta_{w,i}$. At frequencies lower than ω_{th} (~4.2 Hz for the present case), there is a gradual change in $\theta_{w,}$ which happens because the three-phase CL is pinned on the rod surface. However, once the rod rotation speed exceeds $\omega_{th,}$ there is a very steep increase in θ_w until it saturates at a particular value, $\theta_{sat,}$ which, in the case of the present study, is 120° with an uncertainty of ±5°. At such high frequencies, the system occupies a configuration where a thin film of oil is present between the rod and the climbed meniscus (Fig. 4). In such case, θ_w is replaced by $\theta_{app,}$ which is the angle formed at the location of apparent contact between the rod and water–oil interface. Since there is no actual contact of the interface with the rod surface, pinning and CAH cannot occur. This is analogous to the de-pinned CL on the oil-coated rod surface of our previous work related to the rod-climbing effect of

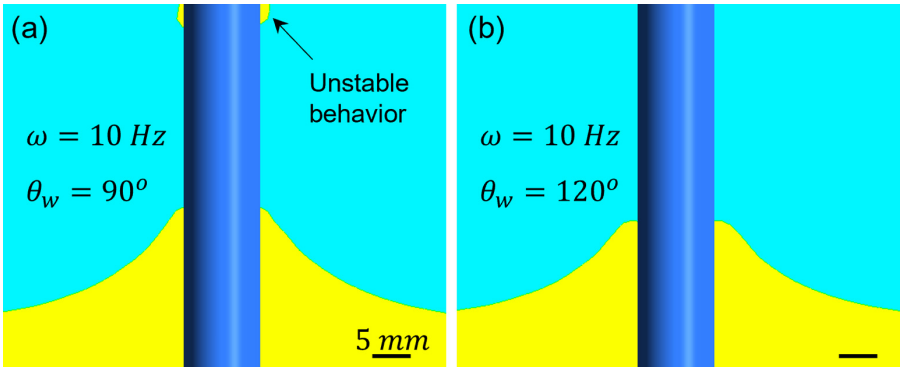

FIG. 12. Configuration of the two liquids obtained from simulation at $\omega = 10$ Hz for (a) $\theta_w = 90°$ (b) $\theta_w = 120°$. Interface shows unstable behavior in the experimental timescale for $\theta_w = 90°$, and the presented figure corresponds to the state after running the simulation for 20 s of physical time. Stable interface is obtained for θ_w=120°.

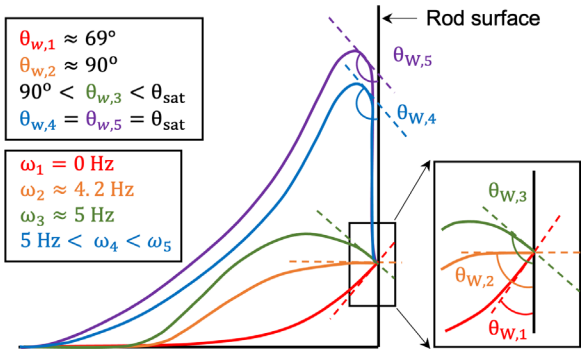

FIG. 13. Schematic showing the interfacial profile and the corresponding contact angle at different rod rotation frequencies. This depicts the mechanism for saturation of contact angle beyond a certain frequency.

viscoelastic liquids.[6] This explains that the contact angle will not change further and assumes a constant saturated value.

D. Discussion on ring instability

As the ω is increased beyond a certain value, ω_{max} (10 Hz for the present case), a steady shape of interface is not observed. The formation of ring instability and water-in-oil emulsion happens at such high rotation frequencies.[1] Figure 14 (Multimedia view) presents the transient evolution of interfacial profile and subsequent emulsification at $\omega = 10.8$ Hz. The process of emulsification begins with the formation of a fingerlike structure [Fig. 14(a)], which starts moving up along the rod with a velocity ~2 mm/s for roughly 3.7 s. This causes the formation of an enclosing sheet of water, referred to as sheet instability by Zhao *et al.*,[2] around the inner thin film of oil [Fig. 14(b)]. Once the fingerlike structure has reached its maximum height, the water sheet persists for ~0.5 s before it breaks up and gets emulsified [Fig. 14(c)]. This causes the uppermost fingerlike structure to get disconnected from the bulk of the water and form a ring-like structure around the rod [Figs. 14(d) and 14(e)]. This is the ring instability as reported by Bonn *et al.*[1] The ring also gets emulsified in a few seconds, and the emulsion gets dispersed into the bulk of the oil. After this, another fingerlike structure forms at the interface and the entire process repeats itself. It is observed that every successive cycle of ring instability and emulsification takes a longer period of time than the previous one (Fig. 14). In the first cycle, the water sheet persisted for ~0.5 s, while in the third cycle, it persisted for more than 40 s. The possible explanation for this observation may lie in the altered hydrodynamic conditions due to increased amount of water-in-oil emulsion, and studying this is beyond the scope of the present work. The method of correcting θ_w in simulations to properly capture the rod-climbing effect of Newtonian liquids as proposed in the present study is applicable only for the regime $\omega \leq \omega_{max}$, where steady-state profile is observed. In this regime, the thin film of oil can be neglected, and the physics can be captured through an apparent contact angle. However, if $\omega > \omega_{max}$, then the simulation with the present parameter cannot be used to supplement the experimental results because the interface no longer reaches a steady state but shows a highly transient and unstable behavior (Fig. 14). Moreover, the $\omega > \omega_{max}$ regime involves emulsification through the breakup of a thin film. This would require a very fine mesh in the simulation to accurately capture this phenomenon, such that it can also account for the thin film of oil and water. Hence, we limit the numerical results of the present study until the regime of angular frequencies $\omega \leq \omega_{max}$ where a steady-state interface exists, and the thin film of oil can be neglected.

V. CONCLUSION

In the present work, we have studied the rod-climbing effect of Newtonian liquids in a stratified system with silicone oil of viscosity 355 mPa s being the lighter liquid and DI water as the heavier liquid. Using a stainless steel rod of diameter 10 mm, steady-state climbing profiles are observed for rotation speeds, ω, up to 10 Hz. Beyond this speed, ring instability and subsequent emulsification are observed. Experiments revealed that the contact angle θ_w at the oil–water–rod interface shows a hysteresis based on the rod rotation speed. To precisely model the Newtonian rod-climbing phenomenon, we propose that the contact angle hysteresis must be accounted in the boundary condition by using the correct value of θ_w at any given ω. The proposed methodology yields a quantitative match between experiments and simulations in terms of climbing height, threshold rod rotation speed, and shape of the oil–water interface. For higher values of ω (>5 Hz), the value of θ_w becomes more than 90° and cannot be measured experimentally due to obstruction from the bulged meniscus. At such high frequencies of rod rotation, a thin film of oil trapped between the rod and the climbed portion of water is also observed. In these cases, the thin film of oil can be neglected and the dynamics of Newtonian rod climbing can be captured in terms of an apparent contact angle, θ_{app}. Using it as a fitting parameter, the value of θ_{app} is obtained from the simulation to match the experimental climbing

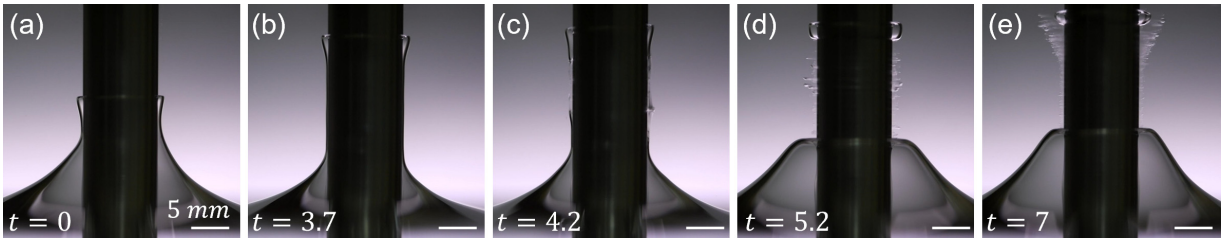

FIG. 14. Transient evolution of interfacial profile at $\omega = 10.8$ Hz. Time is in seconds. The frame at $t = 0$ s corresponds to the initiation of an axisymmetric fingerlike structure. (a) and (b) This structure begins to move along the rod surface at an average velocity of 2 mm/s. (c) At $t = 4.2$ s, the sheet of water breaks down. It gets fully emulsified within a second as can be observed in (d). This causes the fingerlike structure to get disconnected from the bulk fluid, thereby showing a ring instability (d) and (e). Multimedia view: https://doi.org/10.1063/5.0115521.3

height. Reliability of θ_{app} is confirmed by matching the simulated interfacial profile with the experiments. The proposed methodology is applicable only for the ω up to which a steady and stable interface is observed (10 Hz for the present case). Beyond this ω, the proposed method cannot be applied due to the transient nature of the phenomenon and the requirement of a very fine grid size in simulations to account for emulsification assisted by the thin-film breakup.

SUPPLEMENTARY MATERIAL

See the supplementary material for simulation details, deviation of output contact angle from the input value in simulation, and error estimation for the match of experimental and simulated interfacial profile.

ACKNOWLEDGMENTS

All authors acknowledge G. Sai Santhosh Sivan, Project Associate, Department of Mechanical Engineering, Indian Institute of Science Bangalore, for helping with the experimental setup. All authors acknowledge Dr. Udita U. Ghosh, Assistant Professor, Department of Chemical Engineering and Technology, Indian Institute of Technology (BHU) Varanasi, for technical suggestions. N.K.C. acknowledges support from the Prime Minister's Research Fellowship (PMRF). A.K. acknowledges partial support from the office of principal scientific advisor.

AUTHOR DECLARATIONS

Conflict of Interest

The authors have no conflicts to disclose.

Author Contributions

Navin Kumar Chandra: Conceptualization (equal); Data curation (lead); Formal analysis (supporting); Funding acquisition (supporting); Investigation (equal); Methodology (equal); Project administration (supporting); Resources (equal); Software (supporting); Validation (equal); Visualization (lead); Writing – original draft (equal); Writing – review & editing (equal). **Kaustuv Lahiri:** Data curation (equal); Formal analysis (equal); Investigation (supporting); Methodology (supporting); Software (lead); Validation (equal); Visualization (supporting); Writing – original draft (equal); Writing – review & editing (equal). **Aloke Kumar:** Conceptualization (equal); Formal analysis (lead); Funding acquisition (lead); Methodology (equal); Project administration (lead); Resources (lead); Supervision (lead); Writing – original draft (equal); Writing – review & editing (equal).

DATA AVAILABILITY

The data that support the findings of this study are available within the article [and its supplementary material].

REFERENCES

[1]D. Bonn, M. Kobylko, S. Bohn, J. Meunier, A. Morozov, and W. Van Saarloos, "Rod-climbing effect in Newtonian fluids," Phys. Rev. Lett. **93**, 214503 (2004).
[2]C. Zhao, C. Gentric, N. Dietrich, Y. Ma, and H. Z. Li, "Deformation of liquid-liquid interfaces by a rotating rod," Phys. Fluids **29**, 072108 (2017).
[3]J. Dealy and T. Vu, "The Weissenberg effect in molten polymers," J. Non-Newtonian Fluid Mech. **3**, 127–140 (1977).
[4]K. Weissenberg, "A continuum theory of rheological phenomena," Nature **159**, 310 (1947).
[5]D. D. Joseph, G. S. Beavers, and R. L. Fosdick, "The free surface on a liquid between cylinders rotating at different speeds part II," Arch. Rational Mech. Anal. **49**, 381–401 (1973).
[6]N. K. Chandra, U. U. Ghosh, A. Saha, and A. Kumar, "Contact line pinning and depinning can modulate the rod-climbing effect," Langmuir **37**, 14785–14792 (2021).
[7]A. Berman, J. Bradford, and T. Lundgren, "Two-fluid spin-up in a centrifuge," J. Fluid Mech. **84**, 411–431 (1978).
[8]S. Fujimoto and Y. Takeda, "Topology changes of the interface between two immiscible liquid layers by a rotating lid," Phys. Rev. E **80**, 015304 (2009).
[9]W. Zheng, B. Wen, C. Sun, and B. Bai, "Effects of surface wettability on contact line motion in liquid–liquid displacement," Phys. Fluids **33**, 082101 (2021).
[10]L. Liu, L. Wang, H. Song, and M. Bai, "Investigation on influences of polymer solution properties on stress distribution and deformation of residual oil," Eng. Appl. Comput. Fluid Mech. **14**, 401–410 (2020).
[11]R. Fetzer, M. Ramiasa, and J. Ralston, "Dynamics of liquid- liquid displacement," Langmuir **25**, 8069–8074 (2009).
[12]M. Ramiasa, J. Ralston, R. Fetzer, and R. Sedev, "Nanoroughness impact on liquid–liquid displacement," J. Phys. Chem. C **116**, 10934–10943 (2012).
[13]M. Zanini, C. Marschelke, S. E. Anachkov, E. Marini, A. Synytska, and L. Isa, "Universal emulsion stabilization from the arrested adsorption of rough particles at liquid-liquid interfaces," Nat. Commun. **8**, 15701 (2017).
[14]V. Hejazi and M. Nosonovsky, "Contact angle hysteresis in multiphase systems," Colloid Polym. Sci. **291**, 329–338 (2013).
[15]M. Fermigier and P. Jenffer, "An experimental investigation of the dynamic contact angle in liquid-liquid systems," J. Colloid Interface Sci. **146**, 226–241 (1991).
[16]D. Seveno, T. Blake, S. Goossens, and J. De Coninck, "Predicting the wetting dynamics of a two-liquid system," Langmuir **27**, 14958–14967 (2011).
[17]S. Iliev, N. Pesheva, and P. Iliev, "Contact angle hysteresis on doubly periodic smooth rough surfaces in Wenzel's regime: The role of the contact line depinning mechanism," Phys. Rev. E **97**, 042801 (2018).
[18]Q. Liu, J. Yu, and H. Wang, "The role of the substrate roughness in contact angle hysteresis and dynamic deviation," Int. J. Heat Mass Transfer **148**, 118985 (2020).
[19]J. Li and X. Li, "Numerical study of the impact of contact line with hysteresis on the faraday instability," Phys. Fluids **34**, 072108 (2022).
[20]X. Xu and X. Wang, "Theoretical analysis for dynamic contact angle hysteresis on chemically patterned surfaces," Phys. Fluids **32**, 112102 (2020).
[21]N. D. Patil, J. Shaikh, A. Sharma, and R. Bhardwaj, "Droplet impact dynamics over a range of capillary numbers and surface wettability: Assessment of moving contact line models and energy budget analysis," Phys. Fluids **34**, 052119 (2022).
[22]Q. Song, K. Liu, W. Sun, Y. Jiao, Z. Wang, X. Liu, and J. Ye, "Contact angle hysteresis and lateral adhesion strength on random rough surfaces," Phys. Fluids **34**, 082015 (2022).
[23]J. Yang, "Well-posedness of the free surface problem on a Newtonian fluid between cylinders rotating at different speeds," Proc. R. Soc. Edinburgh, Sect. A **2021**, 1–26.
[24]J. U. Brackbill, D. B. Kothe, and C. Zemach, "A continuum method for modeling surface tension," J. Comput. Phys. **100**, 335–354 (1992).
[25]D. D. Joseph, K. Nguyen, and G. S. Beavers, "Non-uniqueness and stability of the configuration of flow of immiscible fluids with different viscosities," J. Fluid Mech. **141**, 319–345 (1984).
[26]D. D. Joseph, Y. Renardy, M. Renardy, and K. Nguyen, "Stability of rigid motions and rollers in bicomponent flows of immiscible liquids," J. Fluid Mech. **153**, 151–165 (1985).